ELSEVIER Journal of Materials Processing Technology 53 (1995) 293–310

Journal of Materials Processing Technology

Hot Working Characteristics Of Steels In Austenitic State

H.J. McQueen,[a] S. Yue,[b] N.D. Ryan[a] and E. Fry[a]

[a]Mech. Eng., Concordia University, Montreal H3G 1M8, Canada

[b]Metal. Eng., McGill University, Montreal, Canada

The behavior of C, HSLA, tool and stainless steels in the austenitic condition during industrial hot forming is reviewed. In the constitutive relations, it is primarily the activation energy which rises with alloy additions. Strain hardening is reduced mainly by dynamic recovery as indicated by its stress dependence and confirmed microscopically in the austenitic stainless steels. Dynamic recrystallization provides additional softening, possible grain refinement and enhanced ductility. After deformation, the metal undergoes static recovery and static recrystallization at longer times to provide grain refinement and stress reduction in any following stage. With rapid cooling, it is possible to retain either hot-work substructures in elongated grains or fine new grains which strengthen the product directly or through refined ferrite.

1. INTRODUCTION

The hot working of steel has spawned extensive and diverse research activities as a consequence both of various compositions and phases and of different process requirements [1-20]. Working in the austenite phase (> $0.6T_M$, melting K), includes low C steel, HSLA (low C) with fine microalloy precipitation, medium C with intermediate alloy contents, tool steels containing considerable alloy carbides and austenitic stainless steels having high solute contents along with segregated δ phase and precipitates. In the ferritic state, where C steels with considerable carbide volume fraction are warm worked and ferritic stainless ones have high levels of solute along with some γ phase, have been reviewed [4, 31-34]. Two phase ($\alpha + \gamma$) working as in duplex stainless steels, in dual phase steels and in intercritical rolling are considered elsewhere [10,11]. The HSLA steels are considerably stronger than C steels and exhibit greatly enhanced grain refinement at low finishing temperatures where microalloy carbonitride precipitation retards restoration mechanisms; however, the application in conjunction with physical simulation and modeling of rolling schedules are discussed elsewhere [8-20]. The austenitic stainless steels provide opportunity for studying dislocation substructures and the progress of dynamic recrystallization (DRX), especially as to how these mechanisms are influenced by solutes and second phase particles [5, 21-30].

The principal mechanism reducing the rate of strain hardening ($\theta = d\sigma/d\varepsilon$) and flow stress σ is dynamic recovery (DRV) which leads to a subgrain structure at all levels of strain $\varepsilon > 0.1$ [31,32, 35-40]. However, at a critical dislocation density (σ_c, ε_c), DRX nucleates and spreads. This additional restoration to DRV causes a flow curve peak (σ_p, ε_p) followed by about 20% work softening to a steady state regime which commences at ε_s, σ_s and also marks the end of the first wave of recrystallization [6,25,29,31,37,40-43]. The DRX is also extremely important

Elsevier Science S.A.
SSDI 0924-0136(95)01987-P

in raising the hot ductility ε_f by halting triple junction cracks initiated by differential grain boundary (GB) sliding [3,6,11,31,38]. Because of the DRV substructure in initial or DRX grains, holding between passes or before cooling causes hot worked metal to undergo static recovery (SRV) and then static recrystallization (SRX) [3,8,9,11-18,25,26,38]. Significant SRX reduces σ in following pass and refines product grain size [8-20].

The presentation commences with a review of constitutive equations (σ dependence on temperature T and strain rate $\dot{\varepsilon}$) and how the constants vary with composition, as well as methods of calculating σ as a function of ε [4,9,10,17,18,23-30,32]. The microstructural evolution with ε as a function of T and $\dot{\varepsilon}$ is discussed by considering the substructure as observed in stainless steels. The dependence of hot ductility on T, ε and composition is explained with a brief examination of the effects of ferrite, carbides, inclusions and insoluble metallic impurities (e.g., Pb, Bi). Static softening is shown to be dependent on T, $\dot{\varepsilon}$ and ε and to be affected by solute and precipitates, notably those formed dynamically.

2. FLOW CURVES AND PEAK STRAINS

The flow curves, as illustrated in Figure 1, are marked by hardening to a peak and softening to a steady state regime at ε_s as a result of DRX which nucleates at $\varepsilon_c \approx 0.7\ \varepsilon_p$ [3-12, 21-31, 48-

Table 1. SOLUTE STRENGTHENING RESULT, SOLUTE RETARDATION PARAMETERS ($2s^{-1}$) AND T_{NR}

ELEMENT	T_{NR}† °C	SRX-SRP	DRX-SRP	SSR	SRX-SRP	DRX-SRP	SSR
		% per 0.1 atom %			% per 0.1 weight %		
			[#$5s^{-1}$]				
Mo in							
Mo steel	880	33 (37*)	25* (23#)	9	20	42	5# (8-9*)
Mo-Nb	940	-	15	10	-	10	6
Mo-V	890	-	-	14	-	-	8
Mo-Nb-V	955	26	20	14	16	13	8
Nb in							
Nb steel	935	(542w) (409*)	135* (124#)	70#	(325w)	92	44# (12.7*)
Nb-Mn		401	-	-	272	-	-
Nb-Mo	940	390	79	100	265	54	63
Nb-V		-	-	80	-	-	50
Nb-Mo-V	955	-	107	90	-	73	56
Nb-Al		(550w)	-	-	(328w)	-	-
V in							
V steel	835	12 (10*)	8.4 (7#)	7	13	9.2	8 (7.9*)
V-Mo	890	-	3.3	11	-	3.6	12
V-Nb		11	-	8	12	-	9
V-Mo-Nb	955	-	5.1	9	-	5.6	10
Ti in							
Ti-1.6 Mn		-	35 (30#)	-	-	42	-
Mn steel		-	-	38	-	-	44
Mn in							
Ti steel		-	3.9 (3#)	2.1#	-	3.9	2.1#
Nb steel		-	2.3	1.3#	-	2.3	1.3#
Al in							
Al steel		(8w)	(13#)	12#	16#	-	-
Al-Nb		(11w)	-	-	38w	-	-
Si in							
γ steel		-	-	0.5#	-	-	0.6#

References: principal[59]; #[55]; †[56]; *[57]; w[60]

50]. Both ε_p and σ_p decrease in a similar manner with rising T and declining $\dot{\varepsilon}$ (but rising $t_p = \varepsilon_p/\dot{\varepsilon}$) [12, 24-26] at the same time as the dislocation density declines and the DRXgrain size becomes larger. Nucleation is retarded by increasingly fast concurrent straining which introduces additional dislocations into the forming nucleus, thus requiring a greater strain energy gradient across the boundary and a smaller cell size [10,25,29, 35-37, 40-42]. At high T and low $\dot{\varepsilon}$ (Figure 1b), multiple peaks occur as the interval ε_x (= ε_s-ε_p)for completion of a wave of DRX becomes shorter than the ε_c for the next wave; this is associated with grain coarsening as explained later [4,24,25,35,42,43].

Flow stress is increased by solute which diminishes DRV, raising the dislocation density through pinning by atmospheres or through reduction in SFE. Fine particles also pin dislocations and stabilize a denser substructure, thus also retarding DRX nucleation [12,18,35,37,40,41]. The peak strain increases with rising solute content and density of fine particles (< 0.5μm) which reduce GB mobility, thereby retarding growth of DRX nuclei [3,12,49,50, 72-74]. The increase in ε_p leads to a rise in σ_p and to a mounting slope in the linear relationship for each alloy (Figure 2) [27,28,48]. An elevated flow curve usually leads to more rapid GB cracking due to higher stress concentration. Likewise, the retardation of DRX indicated by rising ε_p slows down the effective blunting of intergranular cracks and lowers ε_f.

The increase in strength due to solutes has been systematized through the constitutive constants (described later) or through elemental coefficients for microalloying [51-62] and for high alloy contents, such as in low alloy and stainless steels [6,63,64]. In the microalloyed steels, Nb has by far the greatest Solute Strengthening Result (SSR, % per 0.1wt %) namely 44-63 at 2 s^{-1}, the effect being enhanced by simultaneous additions of V and/or Mo (Table 2) [8,18, 53-62]. While Ti has an SSR of 44, V, Mo and Al give rise to only 5 to 12; Mn and Si have very weak effects 3-1. The strengthening effect per atomic % can be correlated with the solute ionic radius, or even better, with the lattice misfit parameter [53-59]. These strengthening factors increase with $\dot{\varepsilon}$ so are expected to be higher for industrial rates of 10 to 100 s^{-1}. The table also shows the Solute Retardation Parameter for DRX (SRP_D), which indicates the increase in ε_p and consequently σ_p, since θ is also raised by the solute influence on substructure [53-60]. Additions of Nb and Ti have effects of 42-92 and hence greatly raise σ_p. Mo has an SRP_D of 42 so that the rise in σ_p is medium compared to the low effects of V and Mn, which have SRP_D less than 10.

Dynamic precipitation also raises the strength at intermediate $\dot{\varepsilon}$ much more than either the

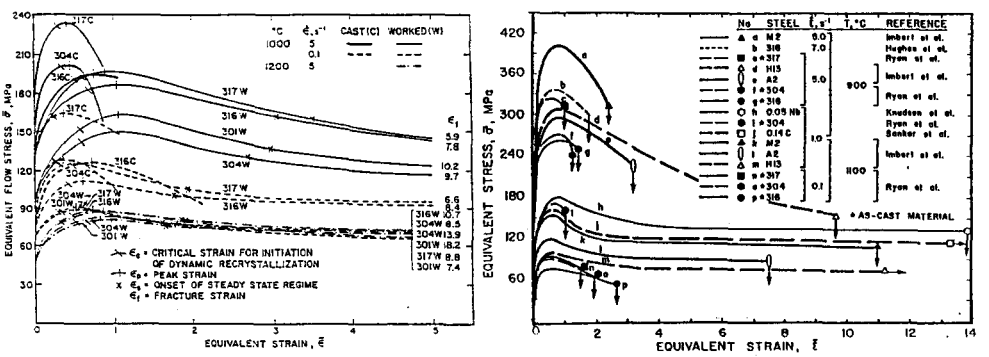

Figure 1: Representative hot working flow curves a) of 301, 304, 316 and 317 showing effects of T, $\dot{\varepsilon}$ and as-cast segregation [22-30] and b) of C, HSLA (fine precipitates) [49], 300 stainless steels (solutes) and tool steels A2, H13 and M2 (coarse carbides) [10,50]. In 317 at 1100°C 0.1s^{-1}, DRX is 30% at ε_p, 70% at 1.5 ε_p, 80% at 2 ε_p and 99% at $\varepsilon_s \approx 3.5\varepsilon_p$.

solute alone at high $\dot{\varepsilon}$ or the precipitates that coarsen in the early stage of deformation at low $\dot{\varepsilon}$. The temperature range depends on the elements: the nose of the PTT (Precipitation-Time-Temperature) curve is at 1000°C for TiC, 900°C for NbCN and 875°C for VCN [59]. The precipitation also retards the occurrence of DRX, which further increases σ_p. The concomitant loss of solute reduces the net hardening and, along with overaging, increases the post peak softening. At high $\dot{\varepsilon}$, DRX is completed and after precipitates raise the steady state stress.

The strengthening effects of element additions up to 5% have been assigned linear coefficients (% per 1wt.%) which decrease as T rises [6,95,96]. At 1000°C, C(-9.4) has a weakening effect, Ni(-0.1) a negligible one, Cr (2.1), a low one, Si and Mn (5.3), medium ones and Mo (13.0) a large one. The average strengthening effect up to large total solute content 40% (sum of wt%) as in 300 series steels is medium (5.0) [6]. However, the 300 series steels with 18Cr - 8Ni as base have a much higher linear increase which depends on the various elements as defined above [95,96]. This results in Mo (0-3%) exerting a total effect equal to Cr (16 - 19%), whereas Ni (8-14%) gives a minor negative effect.

2.1. Flow Curve Calculation

For modeling, it is frequently necessary to know the value of σ as a function of ε as well as of T and $\dot{\varepsilon}$; the common equations are either power functions that are used for cold working with continuous hardening or exponential functions which can predict a peak or saturation stress [4]. Each of these equations have several constants which must be evaluated at different T and $\dot{\varepsilon}$. Flow curves have also been calculated with some success by determining constitutive constants at a series of strain values for the equations in the next section, followed by linear interpolation [17,48,65]. Recently a reduced flow curve equation has been proposed :

$$\sigma/\sigma_p = \varepsilon/\varepsilon_p \, (1 - \exp \varepsilon/\varepsilon_p)^c \qquad (1)$$

which employs σ_p from the constitutive equations and ε_p from a linear dependence on σ_p (Figure 2) [48,66,67]. The value of c is often constant for each alloy (e.g., 0.193 for 316 stainless steel) but may decrease as Z increases. This method is superior to determining constitutive constants at closely spaced strain intervals. This formula does not provide a yield point or stresses beyond ε_p where σ is held constant at σ_p. The latter is not a serious deficiency since in most processing, ε is less than ε_p and in other cases, the overestimation is minor.

3. CONSTITUTIVE EQUATIONS

It has been customary to carry out the constitutive analysis for the peak stress as it represents the upper limit; however the analysis is applicable at a constant ε in cases where the peak is not reached. The power law dependence of σ_p on T and $\dot{\varepsilon}$ ($\dot{\varepsilon} = A' \, \sigma^{n'}$, stress exponent n' is the inverse of the strain rate sensitivity m), which has proven so successful both theoretically and empirically in creep, is not applicable since n' rises with stress [4,5,10,30,66]. The well established equations are the exponential (Eqn. 2) which may be unsuitable at low stresses, and the hyperbolic sine (Eqn. 3-4) (Figure 4) which is actually very similar to the former at high stresses ($\alpha\sigma \geq 1.2$) and to the power law at low stresses ($\alpha\sigma < 0.8$) [4,5,10, 22-30, 39, 67-69]

$$A \text{ " } \exp (\beta\sigma) = \dot{\varepsilon} \exp (Q_{HW}/RT) = Z \qquad (2)$$

$$A \ (\sinh \alpha\sigma)^n = \dot{\varepsilon} \exp (Q_{HW}/RT) = Z \qquad (3)$$

$$\sigma = (1/\alpha) \sinh^{-1} \left\{ \left(\dot{\varepsilon}/\varepsilon_0\right) \exp \left[\left(Q_{HW}/R\right) \left(1/T - 1/T'\right) \right] \right\}^{1/n} \qquad (4)$$

where A, A", α, β (= αn), n, Q_{HW}, T', R (= 8.31 J/mol K) and $\dot{\varepsilon}_0$(= $1s^{-1}$) are constants. The Zener-Hollomon parameter, Z, combines the control variables T and $\dot{\varepsilon}$ and is usually constant in a hot working test and nominally so in many processes. Equation 4 proposed by Tanaka introduces the constant T' ($\approx Q_{HW}/R\ln A$) which does not vary appreciably with composition for a given alloy [30,67]. This discussion is centered on sinh analysis, although exponential analysis has served as the basis for a previous comparison [10]. Similar equations apply to ε_p [12] which is consistent with a linear relationship to σ_p [27,28].

The stress exponent n may have values from 2 to 5, the lower values being associated with higher stresses as observed in HSLA steels. For γ stainless steels, the values in one project embracing 301, 304, 316 and 317 lay in the range 4.2 - 4.6 [24,26,30]. In a compilation from the literature, the average value was found to be 4.3 for all four alloys. The value of n is affected by the choice of α, which has generally been 0.012 M Pa^{-1} for the stainless steels and 0.014 MPa^{-1} for the C and HSLA steels. It is difficult to make comparisons when the α values are greatly different, which explains the use of a common value for the latter two, although a higher α might be more appropriate for the HSLA steels, leading to a higher value of n. The exponent in the sinh law is thus generally much lower than the exponent in the power law, which usually rises considerably above 5 in the high stress regime of hot working [66].

3.1. Activation Energy

In the original Arrhenius theory, the activation energy Q represented the level of an energy barrier to be surmounted in some atomistic mechanism. In high temperature deformation of many metals, the activation energy for secondary creep equals that for self diffusion, leading to the theory that climb of edge dislocations is rate controlling [39,66]. In the case of alloys, especially when DRX is taking place, it has been difficult to associate the Q_{HW} for σ_p with any specific mechanism, since it is usually 20% higher than that for self diffusion in pure metals and is usually much higher than that for GB migration [25]. Almost universally, Q_{HW} increases with alloy content so that one can think of the solute or particles making theoperations of the mechanisms increasingly difficult at lower temperature. The Arrhenius equation fits the trend of

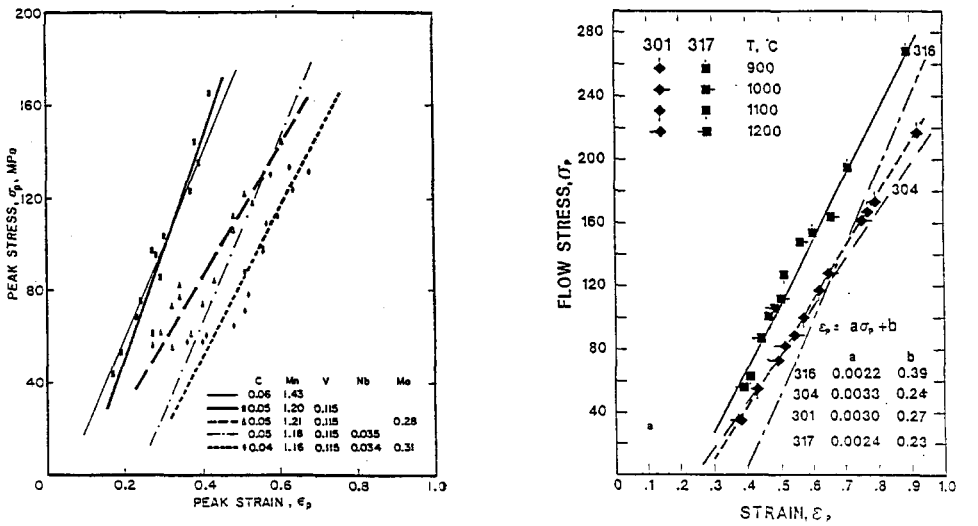

Figure 2: Relationship of peak stress to peak strain is linear, both increasing as T falls and $\dot{\varepsilon}$ rises, for a) C, HSLA steels [48] and b) stainless steels [27,28].

most hot working data and the Q serves as a single value expressing how σ rises as T declines, thus permitting comparison between alloys [10,19]. Q_{HW} for σ_p is higher for alloys partly because ε_p is increasing due to retardation of DRX. Similarly, because ε_p rises as T falls, Q for σ_p is higher than that for σ_i for a fixed ε_i. The Q values for the exponential and sinh laws differ only a little for the same data, so they can be used in comparison of different alloys.

The activation energy of relatively pure iron is about 280 kJ/mol, whereas that of low C steel is approximately 300 kJ/mole as a result of solute strengthening by Mn or Si. The strength and hence the activation energy is not raised by additional completely dissolved carbon, since it enhances diffusion. (The strength and Q for ferritic iron are both lower just below the transformation than those of γ just above [10, 31-33]; however, pearlite exceeding 25% makes both σ and Q greater than those of γ phase until it converts with strain to spheroidal carbides lowering Q [4, 31-33].) The Q_{HW} of HSLA steels (additions < 0.1%) are generally much higher (330 - 450 kJ/mol) than those of C steels because of both solute and formation of microalloy carbonitrides at temperatures between 1000 and 800°C (γ metastable) [48,49]. Data from a high temperature range 1300 to 1000°C (which is not readily available) exhibits a Q_{HW} similar to C steel. Low alloy steels (additions 0.5 - 5%) generally have raised Q_{HW} because of the presence of alloy carbides, strongly affected by variations in the distribution of particles and the distance from equilibrium [33]. For tool steels (additions of 4 - 20%), there are massive carbides around 900°C which progressively dissolve as T rises in a manner depending on composition and structure [10,50]. This can lead to apparent Q_{HW} greater than 500 kJ/mol, but the Arrhenius plots are not linear and can be more reasonably divided into domains associated with differing carbide solubility, thus exhibiting much lower Q_{HW} values at high T.

The activation energies for austenitic stainless steels are much higher (350 - 510 kJ/mol) than for C steels as a result of the high solute content of 28 - 35% for alloys such as 301, 304, 316 and 317 [21-30, 46]. Cr and Mo additions have much greater effect than that of Ni [6,63,64]. Both σ and Q_{HW} are raised by the quantity of δ ferrite retained from the as-cast segregation [23-26, 30]. They can also be raised by high temperature carbides (TiC, TaC) or γ' (Ni_3Al); the variation in σ and Q of these alloys is very similar to that of the Ni-base superalloys [10,31]. Low alloy and tool steels also exhibit solute contributions to strengthening, although the levels are only 5% and 10 - 20% respectively. The constant A is usually determined as the intercepts of plots of log Z versus log (sinh $\alpha\sigma$) in which the single line of data facilitates interpolation to find σ_p for a deformation condition Z. Different melts with the same alloy designation often have the same n and Q but have different strengths expressed as variations in A. Tanaka [67] proposed replacing the preexponential by T' (= Q/R lnA) as shown in Equation 4. T' is much

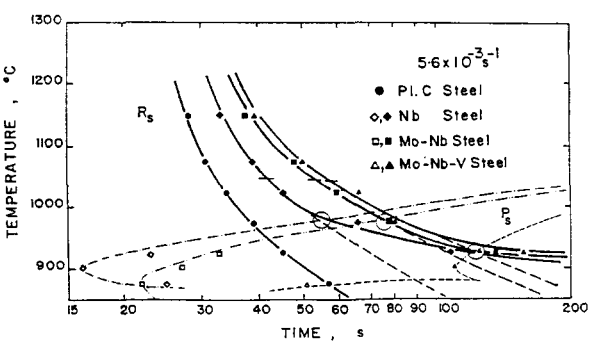

Figure 3: The start of DRX (R_s) is delayed by solutes and by dynamic precipitation start (P_s) in Nb steels, some with additional microalloying [59].

less variable than A because changes in Q_{HW} and A cancel out, especially if determined from a graph of Q_{HW} versus lnA for different batches. A compilation of 70 reports on 300 series steels provides average values of Q_{HW}, n and T' to enable calculation of σ_p for compositions that have not been tested [24,26,30]. The value of Q_{HW} was found to vary linearly with total metallic solute content (MS) [64]. T' generally has a value of about 0.8 T_M [30,67].

The sinh constitutive analysis can be applied to various characteristic points along the flow curve (Figure 4b) [24-26]. The first is for σ_c, ε_c at DRX nucleation, and it has been designated Q_{DRV}. When applied to ε_s, σ_s, at the start of the steady state regime (intersection of softening segment and plateau segment), it is designated Q_{DRX} and is considerably lower than Q_{HW} for the peak because the work softening is greater at lower T. Although this point is the end of the first wave of DRX, Q_{DRX} expresses the T dependence of the flow stress, not that of recrystallization. Elfmark [26,47] proposed this designation and uses it in an equation predicting the fracture strain ε_f. Finally the analysis can be applied to σ_f at ε_f to give Q_f which is used in a predictive equation proposed by Gittins and Sellars [24]. With each of these Q values there are associated values of n which differ slightly from that at the peak.

3.2. θ-σ Analysis

A system of constitutive equations introduced by Kocks and Mecking [17, 71-73] was based on θ ($d\sigma/d\varepsilon$) versus σ curves which descend from a high athermal value more steeply as T rises and $\dot{\varepsilon}$ declines (Figure 5). The underlying theory proposed a dynamic recovery mechanism which altered continuously as T rose from ambient to melting and as $\dot{\varepsilon}$ varied from creep to hot working. In such an analysis of austenitic stainless steels, the changes in curve shape provided information on σ and ε for subgrain formation and for nucleation of DRX, which will be discussed later (Figure 6) [22-26]. From the lower linear θ-σ segment, θ undergoes rapid decline to zero at ε_p; the point of deflection indicates DRX nucleation at ε_c, σ_c. However, extrapolation of this linear segment to θ = 0 provides values of a saturation stress σ_s^* dependent

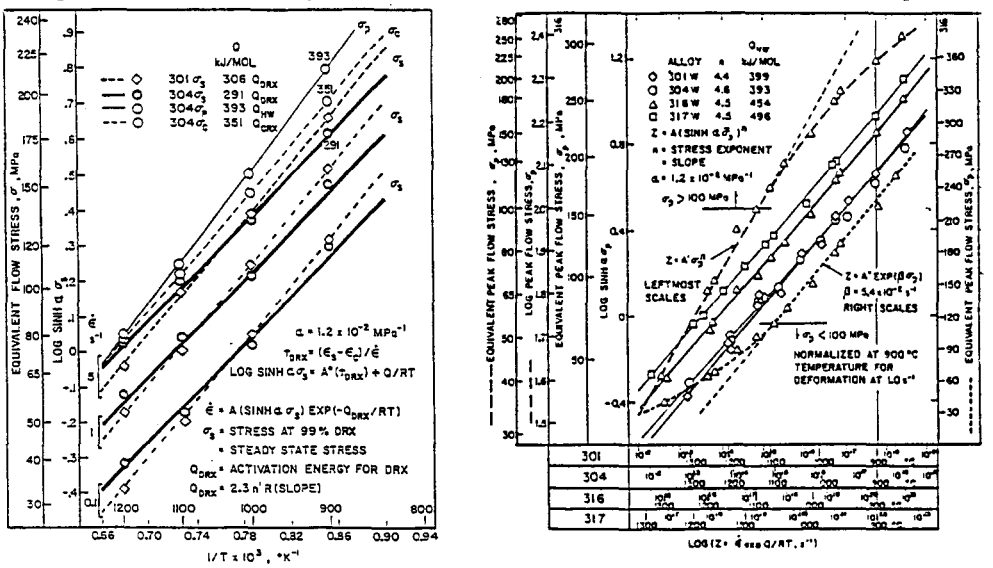

Figure 4: Data on stainless steels plotted according to Equation (3), a) for 301 and 304 critical stress σ_c, peak stress σ_p and steady state stress σ_s and b) for σ_p of 301, 304, 316 and 317 with addition of analyses for power and exponential laws [24-28, 30].

only on DRV which varies from 0.5 to 0.1 of σ at 25°C. The difference between σ_s^* and σ_p or σ_s indicates the softening due to DRX. The activation energy for σ_s^* increases continuously as T rises until 1100°C to become constant at a value similar to that derived from the sinh-Arrhenius analysis [22-26, 72].

The θ-σ analysis was also applied to C and HSLA steels [27] with results similar to those of the stainless steels. One of the expectations of the theory had been to calculate σ-ε curves, which would have been fairly simple if the θ-σ curves had been linear requiring 4 constants. However, the θ-σ curve required approximation by three linear segments each with their constants [A46] so that flow curve calculation was very unwieldy.

4. MICROSTRUCTURES IN DYNAMIC RECOVERY

From optical examination of the prior austenite GB in specimens quenched to martensite, it is possible to see the deformed original grains which are present before the peak of the flow curve or in most hot rolled material. Such observations strongly support DRV as the cause of the reduced strain hardening described above [3,6,17]. Transmission electron microscopy (TEM) of similar elongated grains in stainless steel specimens reveal a subgrain structure with walls which become more regularly organized as T rises (Figure 7) [22-26]. The subgrain size d_s and perfection increase as Z declines and in turn exert a strong influence on σ_s (Figure 8):

$$d_s = e + f \log Z \tag{5}$$

$$\sigma_s = a + b\, d_s^{-1} \tag{6}$$

where a, b, e and f are constants [5,10,21-26,31,32,35-37,39,73-75]. Examination of the dislocation structure as a function of strain shows that tangles form during the initial linear drop in the θ-σ curves. During the transition between linear segments, subgrains form first near the GB and then progressively towards the grain center [28,73]. The second linear segment is related to hardening from additional dislocation storage in the walls.

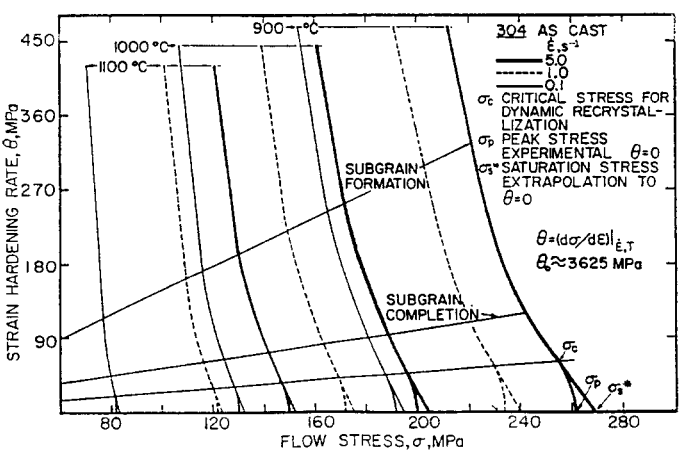

Figure 5: Representative curves of strain hardening θ versus stress up to the peak. As T rises or $\dot{\varepsilon}$ diminishes, the curves displace to lower values of both θ and σ. The curves indicate ε_{SF} (subgrain formation) ε_C (critical for DRX) and ε_f [22-29].

The substructure in γ stainless steels is much more recovered than at room temperature but not as recovered as pure copper or nickel [22-26, 29, 35-38]. Due to the reduction of SFE with increasing solute, the subgrains are better formed in 301 and 304 than in the more highly alloyed 316 and 317. Because of the higher SFE in the plain C-steels without metallic solutes, the level of DRV would be much higher, probably similar to that in pure Ni; the formation of such a substructure is supported by the changes in shape of the θ-σ curves similar to those in the stainless steels and in Cu [22-26, 37,40,74].

The substructure has also been observed in the DRX grains during the steady state regime (Figure 7). The qualitative characteristics are similar to those before the peak. It is difficult to find evidence of dislocation free recrystallized regions, save for an occasional nucleus slightly bigger than the cell size. It would thus appear that the new DRX grains develop substructure rapidly after forming to become indistinguishable from the matrix [22-26, 29,75]. Nevertheless, the DRX does continually reduce the dislocation density, giving rise to the reduction in flow stress. Scanning microscopy (SEM) in channelling mode makes it possible to observe large fields of grains bringing out the distribution in sizes and the presence of substructure by the mottled appearance of the grains [23,25]. The same relationship (Equation 6) between strength and substructure exists before and after the peak [22-26, 37,40,41,75], indicating that the dislocation density defines the flow stress.

5. DYNAMICALLY RECRYSTALLIZED GRAINS

The nucleation of new grains at the original GB just before the peak has been observed in carbon steels (revealed in etched martensite) [41-43] and in stainless steels [5, 22-26, 41,69,77,78]. The growth of these grains into complete necklaces and nucleation of new layers until the old grains are totally transformed is noted during the work softening [17,29,40-43].As a result of such strong dependence on GB nucleation, the rate of DRX is augmented by diminished initial grain size D_0 and consequently ε_p is reduced (σ_p unaltered indicative of a

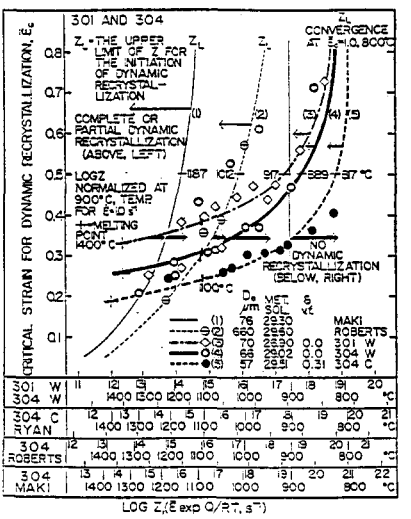

Figure 6: The critical strain for DRX rises with Z to reach a limit beyond which no DRX is possible. ε_C is affected by grain size, particles and solute. For a given ε, the curves may be interpreted as a limiting Z_L, above which there is no DRX and hence no refinement [69].

critical substructure) [3,9, 24-26, 35,36, 40-43]. The presence of almost equiaxed grains containing substructure has been frequently used as conclusive proof of DRX, as distinct from SRX which gives rise to grains without substructure (Figure 9). SEM observations permit large fields of view exhibiting both grains and subgrains by channelling contrast [23]. SRX grains, the few arising from inadequate quenching, stand out due to absence of substructure and presence of twins [98-103].

The average DRX grain size D_S is independent of initial D_0 and remains constant during the steady state regime. This is defined only by the deformation conditions or the stress as in equations 5 and 6 with a set of constants a', b', e' and f' but a grain size exponent near 0.8 (Figure 8) [17, 23-26,35-37,40-43, 69]. The above similarity indicates that the new grains originate from the subgrains (about one in several hundred). Sakai and Jonas [43,79] observed that, under single peak conditions, there was grain refinement whereas, under multiple peak conditions, there was progressive coarsening at each cycle until the stable value was reached [25,41]. Moreover, there is a critical Z_c associated with each D_0 above which grain refinement occurred. The plot of Z_c versus $2D_0$, was found to coincide with the line for Z versus D_S for C and HSLA steels (also stainless[23-26]), showing that there was grain refinement when [79]:

$$2 D_0^{-1} \geq e' + f' \log Z_c \qquad (7)$$

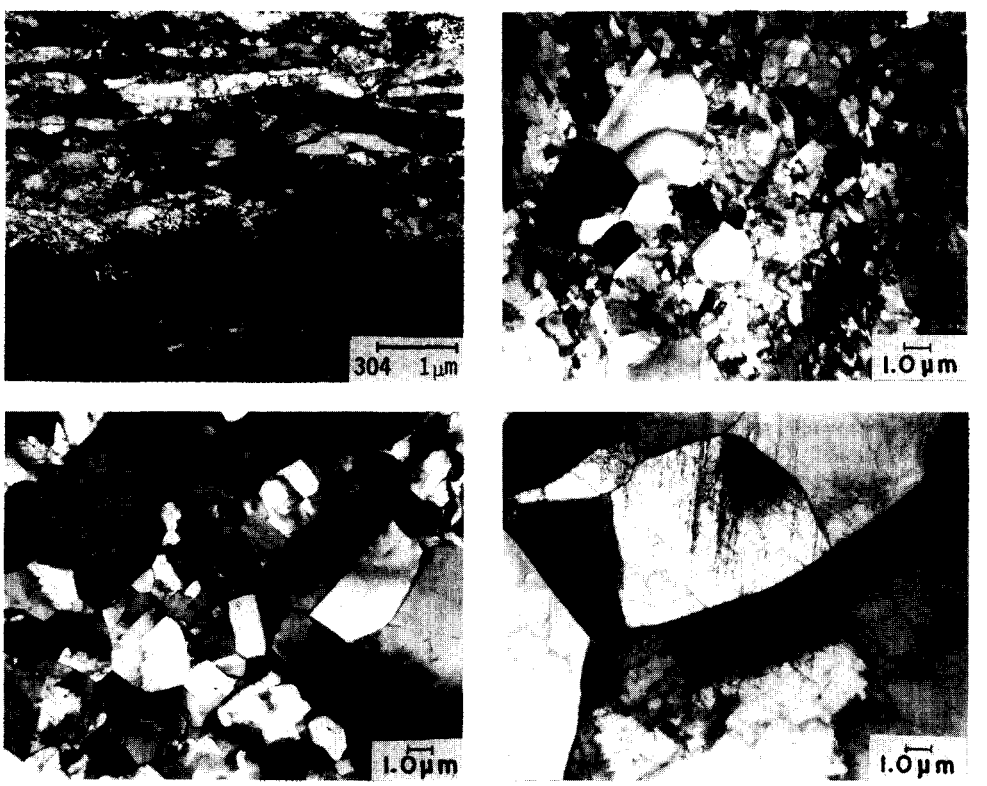

Figure 7: Subgrains become larger and more regular as Z decreases in steady state regime for stainless steels 304 (a) and 317 (b-d) : a) rolled to 80% reduction, no DRX, 820°C, $20s^{-1}$; b) 900°C, $5s^{-1}$, SRX nuclei during cooling; c) 900°C, $0.1s^{-1}$; d) 1100°C, $1.0s^{-1}$ [22-29].

The progress of DRX from optical examination has been shown to follow a modified S curve, since growth starts sharply at the critical strain [19,25]. In addition, the fraction of DRX, X_{DRX}, has been found to follow the Avrami equation developed for SRX :

$$X_{DR} = 1 - \exp(-\beta_D t^{kD}) \quad (8)$$

where t is time and β_D and k_D are constants [17,25,26,69,77,78]. In the 300 series steels, the times for DRX start (t_c $= \varepsilon_c/\dot{\varepsilon}$) and completion ($t_s = \varepsilon_s/\dot{\varepsilon}$) ($\varepsilon_c$ and ε_s from θ-σ and σ-ε curves) were used to locate the Avrami line from which it was possible to calculate the fraction recrystallized along the flow curve (Figure 1a); this was checked by microscopy [17,29,77,78]. From these analyses it has been possible to show how the rate of DRX depends on D_0 and on the dislocation density defined by the flow stress. When the rate was corrected for these factors its true dependence on T could be ascertained so that the Q_{GBM} for GB migration was determined to be 172 kJ/mol, which agrees well with other measurements [25,41].

6. HOT DUCTILITY

The fracture strain ε_f exhibited in a hot forming operation depends both on the stress state induced by the process and on the properties of the material [4,6,11,17,38,44, 80]. If the process has a mean stress (one-third the sum of the principal stresses) less than zero, there is no stress to open cracks and internal voids are welded shut. If the mean stress is positive even if only in a small region due to inhomogeneous deformation, cracking may be initiated. The work piece may have defects which act as stress raisers to initiate cracks; the frequency of these depend on the quality control in prior processing [44]. Failure may also occur due to melting i) of poorly controlled impurity phases, ii) of phases segregated in casting and not removed by homogenization or iii) of slightly segregated regions at the GB, notably when T is raised by deformation heating at high rates either generally or in regions of severe inhomogeneity or strain concentration [17]. In many cases above, fracture is initiated so early that the stress appears unduly low but in other cases (certainly the lattermost), the ductility may be sufficient that the strength is little affected. Finally if none of the above are occurring, which is normal for good quality material, there are inherent fracture mechanisms which are now discussed.

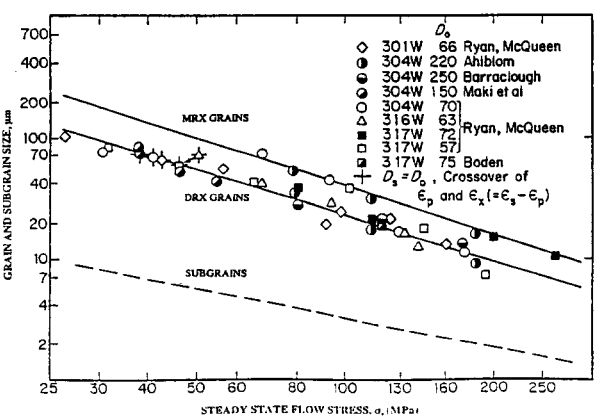

Figure 8: The relation according to Equations 7 and 9 for stainless steels between steady state flow stress and (i) the subgrain size d, (ii) DRX grain size and (iii) MRX grain size after static softening [24-26].

As T is raised into the hot working range ($> 0.5T_M$), GB sliding starts to occur at an increasing rate, relative to the intragranular strain discussed earlier [4-6, 11, 12,17, 22-26,31,38, 44-46]. The proportion of total strain due to sliding decreases as $\dot{\varepsilon}$ increases, so that in an extreme condition, ductile failure occurs as in cold deformation (this is also the case in ferritic steels with low carbide content because of the high level of DRV [31,32]). Although at low $\dot{\varepsilon}$ (~ 0.1 s^{-1}), sliding contributes about one percent of strain, it is sufficient to give rise to cracking at triple junctions due to differential sliding on boundaries under a spectrum of shear stresses. The stress concentrations inducing initiation and propagation are greater if the grains are stronger due to solute or particle effects. However, propagation will be strongly retarded if the GB's migrate away from them as a result of DRX, as will be discussed below. If the mean stress is low, the cracks may propagate considerably along GB's before linking up to cause failure. With large tensile stresses, crack growth is accelerated by plastic flow.

The ductility rises rapidly as T increases further (Figure 10) because augmented DRV softens the grains to lower stress concentrations; in addition, DRX starts at lower ε and proceeds faster [3-6, 11,22-26, 31,35,38,45,80,81]. The ductility also increases as $\dot{\varepsilon}$ rises, partly because GB sliding is relatively diminished and partly because DRX proceeds more rapidly even though it initiates at a higher strain. The ductility is also reduced as the grain size increases because of

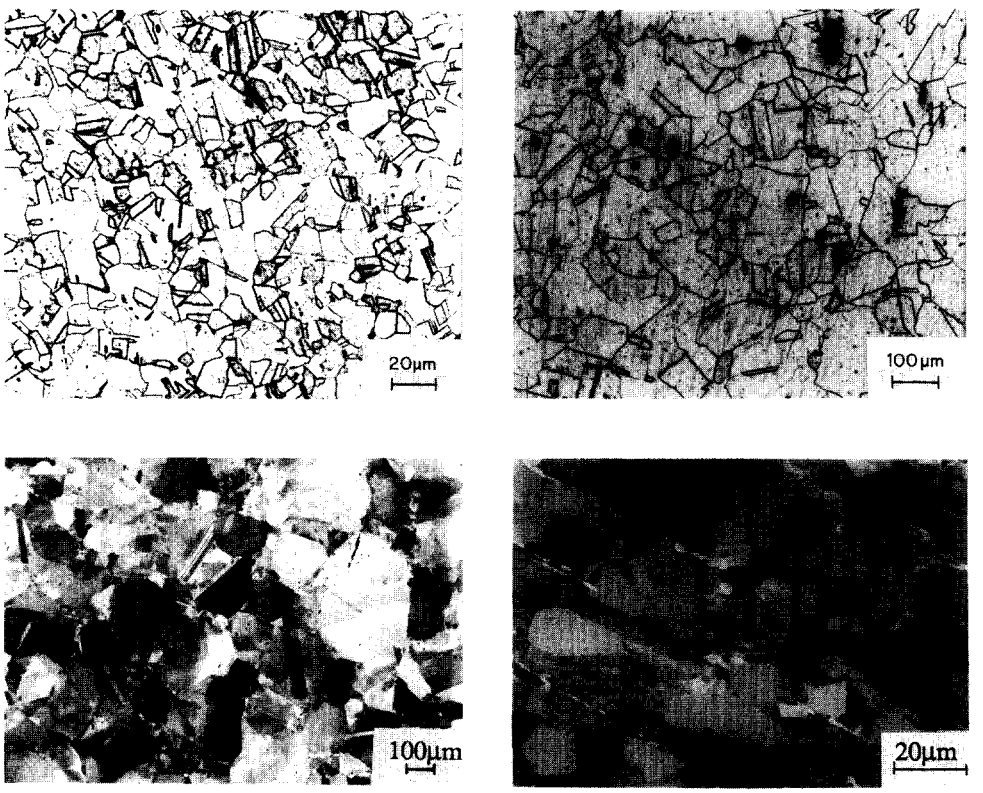

Figure 9: Optical micrographs of 304 torsion specimens showing (a) refined DRX grains at 900°C, 1 s^{-1},and (b) DRX coarsened grains at 1200°C, 0.1 s^{-1}, and SEM channelling mode of 317 as-cast displays subgrains within the grains at 1100°C, 1.0 s^{-1} and mainly SRX grains formed near ferrite stringers at 900°C, 1.0 s^{-1}[22-29].

enlarged crack nuclei; in cases of direct heating to forging T, the ductility may decrease with rising T because the grains become progressively larger [33]. The ductility is increased in multistage testing if the strain per pass is low enough to limit crack formation and if SRX takesplace during the intervals thus eliminating triple junction stress concentrations, separating GB from cracks or producing grain refinement [11,81].

The presence of metallic solutes usually reduces DRV and delays DRX, thus raising σ and reducing ductility. Carbon steels generally exhibit ductility rising with C content due to enhanced DRV, but with an upper limit defined by declining T_M [6,80]. Fine and medium size particles reduce recovery, stabilize substructure to slow nucleation and pin the grain boundaries (at high densities); consequently, they also raise the σ and reduce ductility. Large hard particles (~ 0.6 μm) enhance nucleation but they may also generate additional fissures, leading to a net drop in ductility. The ductility may be reduced by the presence of retained non-equilibrium carbides, depending on their size and distribution, for example being less for pearlite than spheroidite [4,6,33,45,81]. Oxide inclusions, which have a tendency to increase at low C levels, reduce the ductility as additional sources of crack nucleation due either to cleavage, decohesion or void creation by turbulent plastic flow [4-6,10,38,80]. The ability of inclusions to initiate cracks decreases as their size and potential for clustering diminishes [4,44,80]. Moreover, an inclusion may have little effect in certain T ranges if its flow stress becomes less than that of the steel or if it breaks up at very low stresses. Laminar inclusions can cause problems under certain stress conditions and orientations. Certain elements, such as Pb, Bi, S, weaken the GB, greatly enhancing cracking; the problem is solved either by exclusion in processing or by additions to convert them into neutral phases such as MnS [4,6,17,44,80].

The ductility of HSLA steels in reduced considerably relative to that of C steels, notably at T in which precipitation is occurring [4,11,17,49,80]. The fine particles that dynamically precipitate on the dislocations stabilize the substructure, raising σ and retarding nucleation, thus giving more opportunity for cracks to form. Since the steady state regime is dependent on repeated waves of DRX, reduction in their frequency reduces their effectiveness in blunting cracks. Since grain strength is augmented, higher stress concentrations speed up fissure nucleation. In low alloy steels there may be similar problems of carbide precipitation. Moreover, if there is insufficient preheating for equilibrium, large alloy carbide particles may

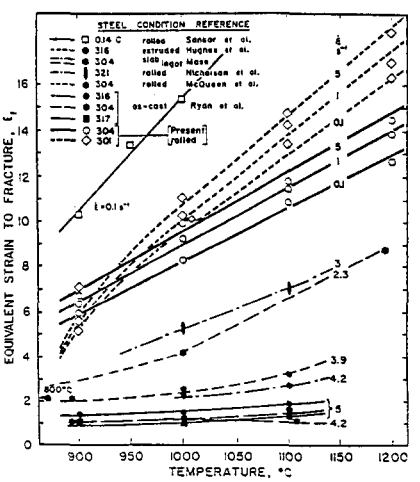

Figure 10: The ductilities of homogenized 301 and 304 increase with rising T and $\dot{\varepsilon}$. They are lower than C steel but higher than as-cast steels or 316 and 321 with more solute [22-29].

initiate fissures. In tool steels, the ductility is augmented in steps as specific carbides dissolve; the effect varies with the ability to reach equilibrium [17,50]. In industrial rolling practice, the work piece is preheated to a T high enough to dissolve carbides while restricting grain growth. During cooling as it is progressively shaped, the influence of the carbides depends on the rate and site of precipitation. The ductility could be much lower on cooling down to the hot forming T than on heating up to it because of precipitation of coarser carbides on reduced GB area [11]. Edge cracking occurring in the "warm" finishing stage becomes the main concern [31].

The ductility of stainless steels depends strongly on the solute level when they are homogenized [5,11, 22-26, 81]. Thus 301 and 304 have high ductilities which improve withrising T and $\dot{\varepsilon}$ (Figure 10). The ductilities of 316 and 317 are markedly lower and decrease with rising $\dot{\varepsilon}$, which enhances stress concentrations more than it reduces GB sliding. Moreover, the ductility of 317 may be reduced by the presence of δ ferrite, which is retained through homogenization. The ductility of the as-cast alloys (-C) is reduced greatly by the quantity and distribution of δ ferrite, which depends on level and type of solutes through their effect on solidification mode and segregation [81]. Ductility is greatly reduced if γ phase nucleates first, since this allows both δ phase and impurities to form on the γ GB's; 316-C proved to have higher ductility than 304-C and 317-C because δ phase is reduced and located at dendrite centers. Nitrogen addition raises the strength and reduces the ductility, notably at lower T [5]. More highly alloyed austenitic stainless steels can be adversely affected by formation of various intermetallic phases on cooling [5]. Since there is no transformation to mask it as in C steels, these γ steels may exhibit a minimum warm ductility, similar to Ni and Cu alloys [11,31,38].

7. STATIC RECRYSTALLIZATION

Static recrystallization (SRX) is likely to take place after hot working during the period that the workpiece remains at a high T; its prevention by rapid cooling is often restricted by workpiece dimensions or process configuration [3,8,9,12-14,18,35,38,82,83]. While loss of retained substructure weakens the product, refined grains give reasonable strength with high ductility for further forming operations. After hot working at a higher T, SRX has a lower

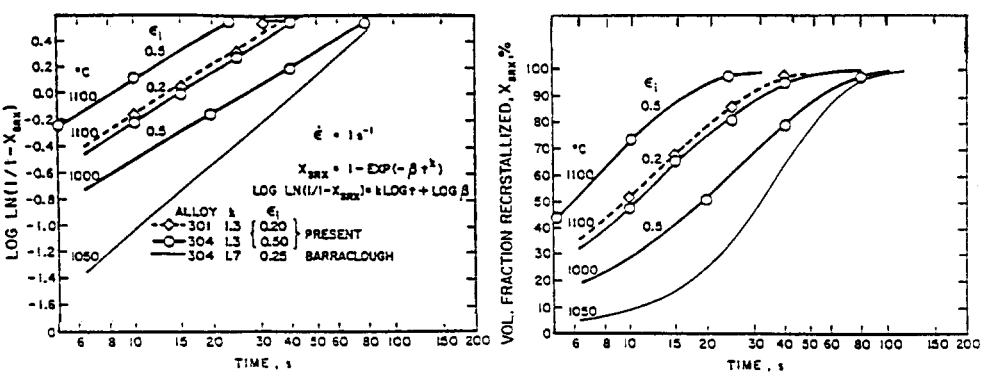

Figure 11: For the volume fraction recrystallized of 301 and 304 versus log t at $\varepsilon = 0.2$ and 0.5, the data form the traditional sigmoidal curves. In addition, an Avrami plot is shown for both alloys. Published data for a large grained steel are included for comparison [77,82,83].

driving force; the strain energy is less than that of a cold work structure which may, however, become degraded during slow heat up in annealing so that it gives rise to greater completion times and grain sizes. Because of the reformed substructure, SRX takes place after DRX mainly by continued growth of DRX nuclei formed just before deformation ends. Such metadynamic recrystallization (MRX) has no incubation and usually produces larger grains than the original DRX ones [9,13,25,35]. However, after high T deformation, there is initially significant static recovery (SRV) [8,9,13,35,38,84].

The progress of SRX can be followed easily by microscopy, if the hot worked product has elongated grains, that is below the critical strain for DRX. Once DRX has taken place, SRX grains can sometimes be distinguished by the freedom of etching artifacts or by the presence of more numerous, straight annealing twins [3,25,35,38]. In stainless steels, SEM in channelling mode clearly exposes the substructure in worked DRX grains and its absence in SRX grains [23,25]; TEM readily distinguishes them also but the field of view is limited [22,23,25]. An effective and expeditious measure is the drop in strength during an interval between two stages of hot deformation [9,13,14,35,38,82-85]. This technique has high accuracy since it avoids disturbance of the specimen and problems of rapid quenching or of phase transformation on cooling so that it can be readily applied to steels [84-86]. The fractional softening (FS) measured involves both SRV and SRX; the amount of each can be distinguished if the entire softening curve is determined [8,12,84,85,87]. As for SRX during annealing after cold working, the Avrami laws (Equation 8) with time exponent k_S of the order of 1.3 for X_{SRX} but about 1.5 for FS as is common when SRV accompanies SRX [8,9,25,27,30,36,82,83] (Figure 11). For MRX, k_S is 1 indicating the absence of incubation [8,9,84].

The time $t_{0.5}$ for SRX and the grain size decrease with a reduction in D_o and with an increase in ε up to the peak; during steady state, D_{SRX} is proportional to D_S thus inversely to Z [12-14, 35,38, 83-86]. Reduction in deformation T, or increase in $\dot{\varepsilon}$ (increase in Z), has a similar effect if the annealing T is constant for fixed ε. However, if the holding T is the same as for deformation, the time for SRX declines with mounting T both for constant stress (rising $\dot{\varepsilon}$) and for constant $\dot{\varepsilon}$ (declining σ) [9,12,13,18,35,38, 83-85]. Recrystallization between stages of deformation is of greater industrial importance than SRX during final cooling [8,9,12,13,17,18,38] for refining the grains, reducing the strength and raising the ductility in subsequent passes. The interpass softening during a rolling schedule with declining T can be evaluated by computation [12,18] or physical simulation by torsion [3,10,11,14,82,83,88-90]. The application to controlled rolling of C and HSLA steels is treated in a sequel [11].

Solid solution or fine particles retard SRX after hot working in a manner similar to that observed after cold working. Such alloying additions have slowed down both DRV and DRX during deformation and consequently have given rise to a higher flow stress. However, the higher driving force for SRX is countered by particle substructure stabilization or by reduced GB mobility due to particle pinning and solute drag [8,18,35,38,40]. In stainless steels [92,93,98,99], the metallic solute levels range from 25 to 35% and consequently retard SRX substantially in comparison to C steels, where increase in dissolved C has only a small effect [13,35,94]. The activation energies for SRX are 30 to 60% higher than for C steels. The time between hot rolling passes must be lengthened if complete softening and grain refinement is desired. On the other hand, it is comparatively easy to retain the substructure after a cool finishing pass in order to strengthen the product by as much as 20% [5,21,81]. In simple C steels and Ni-Cr steels, additional C augments DRV and reduces the flow stress if it is in solution; however, in steels where alloy carbides form, there is an opposite effect. In HSLA steels, the microalloying elements in solution have significant effects but precipitation retards SRX for a much longer time having industrial importance in producing fine-grained products [3,8,12,17,18,35,51-62]. The microalloy carbonitrides precipitate very rapidly on substructures, especially dynamically during deformation [13,18,31,37, 51-53].

11. CONCLUSIONS

Beneath the diversity of steel microstructures and industrial hot forming processes, there is a fundamental behavior characteristic of the austenitic state. The strain hardening is lowered as dynamic recovery rises with temperature; the consequently reduced flow stress lowers the incidence of grain boundary cracking induced by the sliding at high temperatures. At higher strains, dynamic recrystallization produces new grains that give rise to the flow-curve peak and to work softening. In the final steady state regime, the stress depends on the dynamically recovered substructure that forms in the repeatedly recrystallized grains. Dynamic recrystallization extends the ductility by separating grain boundaries from fissures, thus halting their propagation. Due to the substructure at all stages ($\varepsilon_i > 0.05$), static recrystallization is capable of nucleating rapidly either at the deformation temperature after working or during cooling. During interpass delays, it is of great industrial consequence since it leads to reduced flow stress in the following pass, refinement of the grains and increased ductility.

REFERENCES

1. W.L. Roberts, The Hot Rolling of Steel, Marcel Dekker Publishers, New York, 1983.
2. I. Tamura, C. Ouchi, T. Tanako and H. Sekine, Thermomechanical Processing of High Strength Low Alloy Steels, Butterworths, London, 1988.
3. C. Rossard, in: Microstructure and Design of Alloys, ICSMA 3, Inst. Metals, London, 1973, Vol. 2, pp. 175-203.
4. C.M Sellars and W.J. McG. Tegart, Int. Metall. Rev., 17 (1972) 1-24.
5. B. Ahlblom and R. Sandstrom, Int. Metall. Rev., 27 (1982) 1-27.
6. W.J.McG. Tegart and A. Gittins, in: J.B. Ballance, (Ed.), The Hot Deformation of Austenite, TMS-AIME, Warrendale, PA, 1977, pp. 1-46.
7. G.E. Dieter, Workability Testing Techniques, ASM, Materials Park, OH, 1984.
8. J.J. Jonas, in: Proc. 4th Int. Conf. Strength of Metals and Alloys, ENSMIN Nancy, 1976, pp. 976-1002.
9. W. Roberts in: H.J. McQueen et al., (Eds.), Strength of Metals and Alloys, Pergamon Press, Oxford, 1985, Vol. 3, pp. 1859-1892.
10. N.D. Ryan and H.J. McQueen, J. Mech. Working Tech., 12 (1986) 279-296, 323-349.
11. H.J. McQueen, S. Yue, N.D. Ryan and E. Fry, Proc. XIV Intnl. Conf. Advanced Materials Technologies, Zakopone, 1995, L.A. Dobrzanski, (Ed.).
12. C.M. Sellars, in: C.M. Sellars and G.J. Davies, (Eds.), Hot Working and Forming Processes, Metals Society, London, 1980, pp. 3-15.
13. H.J. McQueen, M.G. Akben and J.J. Jonas, in: N.H. Anderson et al., (Eds.), Microstructural Characteristization By Non-Microscopic Techniques, Riso Natl. Laboratory, Roskilde, Denmark, 1984, pp. 397-403.
14. H.J. McQueen, Can. Metall. Q., 21 (1982) 445-460.
15. C. Rossard and P. Blain, in: Flat Rolled Products III, Met. Sci. Conf. 16, Gordon and Breech, New York, 1962, pp. 3-28.
16. W.J. McG. Tegart, Metals Australia, 3 (1) (1971) 3-8.
17. C.M. Sellars, in: G. Krausz, (Ed.), Deformation Processing and Structure, ASM, Metals Park, OH, 1983, pp. 245-278.
18. W. Roberts, in: G. Krausz, (Ed.), Deformation, Processing and Microstructure, ASM, Metals Park, OH, 1983, pp. 109-184.
19. H.J. McQueen, J. Mat. Proc. Tech. 37 (1993) 3-36.
20. J.J. Jonas and C.M. Sellars, in: J.A. Charles et al., (Eds.), Sir Robert Honeycombe

Commemorative Symposium, Inst. Materials, Royal Society, London, 1992,pp.147-177.
21. H.J. McQueen, E. Evangelista and N.D. Ryan, in: W. Nicodemi, (Ed.), Processes and Material Technology, Stainless Steel 1993, (Florence), Assoc. Ital. Metal, Milan, 1993, Vol. 2, pp. 289-302.
22. H.J. McQueen, N.D. Ryan and E. Evangelista, Mat. Sci. Eng., 81 (1986) 259-272.
23. E. Evangelista, N.D. Ryan and H.J. McQueen, Met. Sci. Tech., 5 (1987) 50-58.
24. N.D. Ryan and H.J. McQueen, High Temp. Tech., 8 (1990) 27-44.
25. N.D. Ryan and H.J. McQueen, High Temp. Tech., 8 (1990) 185-200.
26. N.D. Ryan and H.J. McQueen, J. Mat. Proc. Tech., 20 (1990) 177-199.
27. A. Cingara and H.J. McQueen, J. Mat. Proc. Tech., 36 (1992) 17-30, 31-42.
28. H.J. McQueen, A. Cingara and N.D. Ryan, Mat. High Temp., 10 (1992) 201-206.
29. H.J. McQueen, Y. Cui, B. Li, Q. Meng and N.D. Ryan, in: N.D. Ryan et al., (Eds.), Strip Casting, Hot and Cold Working of Stainless Steel, Met. Soc. CIMM, Montreal, 1993, pp. 181-192.
30. N.D. Ryan and H.J. McQueen, in: Stainless Steels '87, Inst. of Metals, London, 1987, pp. 498-507.
31. H.J. McQueen and D.L. Bourell, J. Met., 39 [7] (1987) 28-35.
32. D.L. Bourell and H.J. McQueen, J. Mat. Shaping Tech., 5 (1987) 53-73.
33. T.Matuszewski,P.M.Machmeier and H.J.McQueen,Metall. Trans., 22A, 1991, 469-497.
34. N.D. Ryan, C. Imbert and H.J. McQueen, in: N.D. Ryan et al., (Eds.), Strip Casting, Hot and Cold Working of Stainless Steel, Met. Soc. CIMM, Montreal,1993, pp.165-180.
35. H.J. McQueen and J.J. Jonas, in: R.J. Arsenault, (Ed.), Plastic Deformation of Materials, Treatise on Mat. Sci. Tech., 6, Academic Press, New York,1975, pp.393-493.
36. H. Mecking and G. Gottstein, in: F. Haessner, (Ed.), Recrystallization of Metallic Materials, Dr. Reiderer Verlag Stuttgart, 1977, pp. 195-212.
37. H.J. McQueen and J.J. Jonas, J. Appl. Metal Working, 3 (1984) 233-241.
38. H.J. McQueen and J.J. Jonas, J. Appl. Metal Working, 3 (1985) 410-420.
39. H.J. McQueen, in: T.G. Langdon et al., (Eds.), Hot Deformation of Aluminum Alloys, TMS-AIME, Warrendale, PA, 1991, pp. 31-54.
40. H.J. McQueen, Mat. Sci. Eng., A101 (1987) 149-160.
41. H.J. McQueen, E. Evangelista and N.D. Ryan, in: T. Chandra, (Ed.), Recrystallization ('90) in Metals and Materials, TMS-AIME, Warrendale, PA, 1990, pp. 89-100.
42. C.M. Sellars, Phil. Trans. R. Soc. London, A288 (1978) 147-158.
43. T. Sakai and J.J. Jonas, Acta Metall., 32 (1984) 189-209.
44. H.J. McQueen, in: G. Sih and C.J. Provan, (Eds.), Defects, Fracture and Fatigue, Martinus Nicholt Pub, The Hague, 1983, pp. 459-471.
45. H.J. McQueen, J. Bowles and N.D. Ryan, Microstruc. Sci., 19 (1989) 357-373.
46. N.D. Ryan and H.J. McQueen, in: A.S. Krausz et al., (Eds.), Constitutive Laws of Plastic Deformation and Fracture, Kluwer Academic Pub., Dordrecht, 1990, pp.333-340.
47. J. Elfmark, Czech J. Phys., B35 (1985) 269-274.
48. H.J.McQueen, O.Overdal, A.Cingara H.Gjestland, Mat. High Temp.,10,1992,207-218.
49. J. Sankar, D. Hawkins and H.J. McQueen, Metall. Tech., 6 (1979) 325-331.
50. C. Imbert, N.D. Ryan and H.J. McQueen, Metall. Trans., 15A (1984) 1855-1864.
51. I. Weiss and J.J. Jonas, Metall. Trans., 10A (1979) 831-840.
52. T. Chandra, I. Weiss and J.J. Jonas, Met. Sci., 16 (1982) 97-104.
53. M. G. Akben, I. Weiss and J.J. Jonas, Acta Metall., 29 (1981) 111.
54. J.-P. Michel, M.G. Akben and J.J. Jonas, Rev. Metall. CIT, 78 (1981) 823-833.
55. M.G. Akben, T. Chandra, P. Plassiard and J.J. Jonas, Acta Metall., 32 (1984) 591-602.
56. B. Bacroix, C. G'Sell, M.G. Akben and J.J. Jonas, Acta Metall., 31 (1983) 619-629.
57. L.H. Andrade, M.G. Akben and J.J. Jonas, Metall. Trans., 14A (1983) 1967-1977.

58. J.J. Jonas and M.G. Akben, Metals Forum, 4 (1981) 92-101.
59. M.G. Akben and J.J. Jonas, in: Int. Conf. Technology and Applications of HSLA Steels, ASM, Metals Park, OH, 1984, pp. 149-161.
60. G.L. Wang and M.G. Akben, in: A.J. DeArdo, (Ed.), Processing, Microstructure and Properties of HSLA Steels, TMS, Warrendale, PA, 1988, pp. 79-89.
61. W.J. Liu and J.J. Jonas, in: A.J. DeArdo, (Ed.), Processing, Microstructure and Properties of HSLA Steels, TMS, Warrendale, PA, 1988, pp. 39-49.
62. T. Mavropoulos, J.J. Jonas and G.E. Ruddle, in: J.M. Gray et al., (Eds.), HSLA Steels 85, (Beijing), ASM, Metals Park, OH, 1986, pp. 229-234.
63. H.J. McQueen and N.D. Ryan, in: D.G. Brandon et al. (Eds.), Strength of Metals and Alloys, ICSMA 9, Freund Publishing House, London, 1991, pp. 359-366.
64. M. Zidek and B. Kubickova, Tech. Digest, 3 (1968) 154-161.
65. K.P.Rao,E.B.Hawbolt,H.J.McQueen and D.Baragar,Can.Metall. Q.,32, 1993,165-175.
66. H.J. McQueen, W. Blum, Q. Zhu and V. Demuth, in: T.R. Bieler et al., (Eds.), Advances in Hot Deformation Textures and Microstructures, TMS-AIME, Warrendale, PA, 1993, pp. 235-250.
67. K. Tanaka, T. Nakamura, Y. Hoshida and S. Hara, Res. Mech., 12 (1986) 41-57.
68. T. Sheppard, in: J.Jeglitsch et al., (Eds.), Proc. 8th Light Metal Congress, The University, Leoben, 1987, pp. 301-311.
69. N.D. Ryan and H.J. McQueen, Can. Metall. Q., 29 (1990) 147-162.
70. A. Gittins and C.M. Sellars, Metal Sci., 6 (1972) 118-122.
71. H. Mecking, B. Nicklas, N. Zarubova and U.F. Kocks, Acta Metall., 34 (1986) 527.
72. N.D. Ryan and H.J. McQueen, in: D.G. Brandon et al., (Eds.), Strength of Metals and Alloys, ICSMA 9, Freund Publishing House, London, 1991, pp. 675-682.
73. G. Carfi, C. Perdrix, D. Bouleau and C. Donadille, in: H.J. McQueen et al., (Eds.), Strength of Metals and Alloys, ICSMA 7, Pergamon Press, Oxford, 1985, pp. 929-934.
74. P. Choquet, B. de Lamberterie and C. Perdrix and H. Blausser, in: B. Fazan et al., (Eds.), Proc.4th Steel Rolling Congress, IRSID,Mazieres-Le-Metz, France,1987,B5.1-8.
75. L. Fritzmeier, M.J. Luton and H.J. McQueen, in: P. Haasen et al., (Eds.), Strength of Metals and Alloys, ICSMA 5, Pergamon Press, Oxford, 1979, pp. 95-100.
76. S.V. Raj and G.M. Pharr, Mat. Sci. Eng., 81 (1986) 217-237.
77. D.R. Barraclough and C.M. Sellars, Metal Sci., 13 (1979) 257-267.
78. W. Roberts and B. Ahlblom, Acta Metall., 26 (1978) 801-813.
79. T. Sakai, M.G. Akben and J.J. Jonas, Acta Metall., 31 (1983) 631-642.
80. A. Gittins and W.J.McG. Tegart, Metal Forum, 4 (1981) 57-62.
81. N.D. Ryan and H.J. McQueen, in: R.A. Lula (Ed.), New Developments in Stainless Steel Technology, ASM, Materials Park, OH, 1985, pp. 293-304.
82. N.D. Ryan and H.J. McQueen, Materials Forum (Australia), 14, (1990) 283-295.
83. N.D. Ryan and H.J. McQueen, Mat. Sci. Tech., 7, (1991), 818-826.
84. R.A. Petkovic, M.J. Luton and J.J. Jonas, Can. Metall. Q., 14 (1975) 137-145.
85. M.G. Luton, R. Dorvel and R.A. Petkovic, Metall. Trans., 11A (1980) 411-420.
86. H.Weiss, D.H. Skinner and J.R. Everett, J.Phys. E., (Sci. Instrum.), 6 (1973) 709-714.
87. A. Sandberg and D. Sandstrom, Mat. Sci. Tech., 2 (1986) 917-937.
88. N.D. Ryan and H.J. McQueen, Can. Metall Q., 30 (1991) 113-124.
89. N.D. Ryan and H.J. McQueen, J. Mat. Proc. Tech., 36 (1993) 103-123.
90. H.J. McQueen and N.D. Ryan, in: N.D. Ryan et al., (Eds.), Strip Casting, Hot and Cold Working of Stainless Steel, Met. Soc. CIMM, Montreal, 1993, pp. 91-106.
91. F.H.Samuel, S. Yue, J.J. Jonas and B.A. Zbinden, ISIJ Intl., 29 (1989) 878-886.
92. L.H. Pussegoda, S. Yue, J.J. Jonas and P.J. Hunt, in: HSLA Steels 90, (Beijing), TMS-AIME, Warrendale, PA, 1992, pp. 159-163.